photonics

MDPI

Article

Silicon-Thickness-Dependent Optimization of Ultra-Thin SOI Graphene–Plasmonic Slot Electro–Optic Modulators

Amr G. AbdElKader [1,2,*] and Kazutoshi Kato [1]

[1] Graduate School of Information Science and Electrical Engineering, Kyushu University, Fukuoka 819-0395, Japan
[2] Faculty of Engineering, Alexandria University, Alexandria 21544, Egypt
* Correspondence: abdelkader.amr.026@m.kyushu-u.ac.jp

Abstract

Graphene–plasmonic electro–optic (EO) modulators have attracted significant interest for compact and energy-efficient integrated photonic systems due to their electrically tunable optical response and strong light–matter interaction. In this work, an ultra-thin silicon-on-insulator (SOI) graphene–plasmonic slot modulator (G-PSM) is investigated using a combined semi-analytical and numerical framework. The analysis integrates finite-temperature Kubo conductivity modeling, perturbation-based effective-index analysis, overlap-factor evaluation, eigenmode analysis, and full-wave simulations to study the influence of silicon thickness on the EO performance of the proposed structure. The obtained results demonstrate that geometry engineering strongly affects modal confinement, overlap enhancement, effective-index perturbation, transmission characteristics, extinction ratio (ER), insertion loss (IL), energy-per-bit consumption, and EO bandwidth. Under optimized operating conditions, the proposed G-PSM achieves an effective refractive-index variation of approximately 3.1×10^{-3}, an ER of approximately 3.5 dB, an IL of 1.5–2 dB, an energy-per-bit consumption of approximately 7.5 fJ/bit, and a 3 dB EO bandwidth approaching 200 GHz. Strong electromagnetic confinement is achieved inside the plasmonic slot region near the graphene-active layer, enabling efficient electro–absorptive and electro–refractive modulation. Excellent agreement between the semi-analytical calculations and numerical simulations validates the developed framework and confirms the suitability of the proposed ultra-thin SOI G-PSM for compact broadband EO modulation in future integrated photonic systems.

Keywords: graphene–plasmonic slot modulators; hybrid plasmonic waveguides; ultra-thin silicon-on-insulator platforms; photonic integrated circuits; graphene conductivity tuning; geometry-engineered EO modulation; electro–absorptive modulation; electro–refractive modulation; modal confinement enhancement; broadband integrated photonics

Check for updates

Received: 22 May 2026
Revised: 9 June 2026
Accepted: 12 June 2026
Published: 14 June 2026

Copyright: © 2026 by the authors. Licensee MDPI, Basel, Switzerland. This article is an open access article distributed under the terms and conditions of the Creative Commons Attribution (CC BY) license.

1. Introduction

In this section, the background and motivation underlying thickness-engineered graphene–plasmonic electro–optic (EO) modulators are first introduced in Section 1.1, followed by a discussion of the current state of the art and the corresponding research gap in Section 1.2. Subsequently, the principal contributions and scientific significance of the present work are summarized in Section 1.3 to emphasize the role of silicon-thickness engineering in enhancing the EO performance of ultra-thin SOI hybrid modulation platforms.

1.1. Background and Motivation

The growing demand for compact, high-speed, and energy-efficient photonic integrated circuits (PICs) has intensified interest in EO modulators with enhanced modulation efficiency and reduced device footprint [1]. Although silicon photonics provides excellent Complementary Metal–Oxide–Semiconductor (CMOS) compatibility and large-scale integration capability [2], conventional silicon EO modulators suffer from the weak plasma-dispersion effect, which limits modulation efficiency and typically requires long interaction lengths [3].

Graphene has emerged as a promising active material for EO modulation due to its electrically tunable optical conductivity, ultrafast carrier dynamics, and broadband optical response [4,5]. Through electrostatic biasing, the graphene chemical potential (μ_c) can be dynamically controlled, enabling efficient electro–absorptive and electro–refractive modulation [6]. Recent review articles have highlighted the rapid development of graphene-based EO modulators for integrated photonic applications, emphasizing their potential for high-speed operation, broadband functionality, and low-power optical signal processing [7]. Meanwhile, plasmonic slot waveguides provide strong subwavelength electromagnetic confinement, significantly enhancing light–matter interaction near the graphene-active region [8]. Consequently, hybrid graphene–plasmonic slot architectures offer considerable potential for realizing ultra-compact EO modulators with improved modulation performance [9].

In silicon photonics, the term ultra-thin SOI generally refers to silicon guiding layers with thicknesses substantially smaller than the standard 220 nm SOI platform commonly employed in integrated photonic devices. Typical ultra-thin SOI configurations utilize silicon thicknesses (t_{Si}) below approximately 150 nm, enabling stronger control over modal confinement and enhanced interaction between the guided optical mode and surrounding active materials. Accordingly, the t_{Si} range investigated in this work (80–140 nm) lies within the ultra-thin SOI regime and is particularly suitable for graphene–plasmonic EO modulation.

Plasmonic waveguiding structures have emerged as a powerful platform for overcoming the diffraction-limited confinement of conventional dielectric waveguides by concentrating optical fields into deeply subwavelength regions. Such enhanced electromagnetic confinement can substantially strengthen light–matter interactions, thereby improving the efficiency of EO modulation, optical sensing, and nonlinear photonic processes. In graphene-assisted plasmonic devices, the strong field localization provided by metallic slot structures increases the overlap between the optical mode and the electrically tunable graphene layer, enabling enhanced modulation efficiency within compact device footprints. Recent reviews have further highlighted the growing importance of plasmonic and hybrid photonic architectures for next-generation integrated photonic systems and advanced functional materials [10,11].

Despite recent progress, the influence of geometry engineering on EO performance in ultra-thin SOI graphene–plasmonic slot modulators (G-PSMs) remains insufficiently explored. In particular, t_{Si} and plasmonic slot width (w_{slot}) strongly affect modal confinement, overlap factor, effective-index variation, transmission characteristics, extinction ratio (ER), insertion loss (IL), EO bandwidth, and energy consumption. Therefore, this work presents a geometry-dependent investigation of an ultra-thin SOI G-PSM using a combined semi-analytical and numerical framework in order to identify favorable operating conditions for compact and broadband EO modulation.

1.2. Related Works and Research Gap

Recent studies have demonstrated significant progress in graphene-assisted EO modulators based on SOI platforms, plasmonic slot waveguides, and hybrid integrated photonic structures [12–14]. These structures exploit the electrically tunable conductivity of graphene together with strong plasmonic confinement to enhance light–matter interaction within compact device dimensions.

A comprehensive review of silicon-based graphene EO modulators highlighted the advantages of graphene integration in enhancing modulation efficiency, reducing device footprint, and enabling high-speed operation [12]. However, their work primarily focused on the classification, operating principles, and performance characteristics of existing graphene modulators rather than geometry-dependent optimization of graphene–plasmonic structures. Similarly, previous studies on graphene-assisted plasmonic devices have emphasized enhanced light–matter interaction through plasmonic confinement and graphene conductivity engineering. Nevertheless, these investigations mainly focused on material properties, plasmonic enhancement mechanisms, or device-specific optimization strategies without systematically examining the role of ultra-thin SOI thickness engineering [15]. Furthermore, while several reported structures investigated the effects of graphene biasing, resonator design, or slot-waveguide configurations, the combined influence of t_{Si}, plasmonic-slot confinement, and electrically tunable graphene conductivity on device-level EO performance metrics remains insufficiently understood.

Despite these advances, most reported works mainly focus on graphene conductivity tuning, wavelength-dependent operation, or plasmonic confinement enhancement, while geometry-dependent EO optimization remains comparatively underexplored. Building upon the limitations identified in the existing literature, the influence of geometrical design parameters on overall device-level EO performance remains comparatively underexplored, particularly for ultra-thin SOI graphene–plasmonic slot architectures. While previous studies have examined graphene conductivity tuning, resonator optimization, or plasmonic confinement enhancement individually, the combined influence of t_{Si} engineering and electrically tunable graphene conductivity has not yet been systematically investigated in G-PSMs [16].

In addition, many existing studies rely primarily on numerical simulations without establishing a physically interpretable framework capable of correlating conductivity evolution, modal overlap enhancement, effective-index modulation, and device-level EO performance under different geometrical conditions.

Therefore, the main research gap addressed in this work is the absence of a systematically validated geometry-dependent optimization framework for ultra-thin SOI G-PSMs capable of correlating t_{Si} engineering with modal confinement, effective-index modulation, transmission behavior, ER, IL, and EO performance tradeoffs.

1.3. Main Contributions and Novelty

This work presents a geometry-dependent investigation of an ultra-thin SOI G-PSM using a combined semi-analytical and numerical framework. Unlike previous studies mainly focused on conductivity tuning or fixed geometrical configurations, the present work systematically examines the influence of t_{Si} on modal confinement and EO performance. The main contributions are summarized as follows:

- A geometry-engineered G-PSM architecture is investigated to analyze the influence of ultra-thin SOI confinement and plasmonic slot dimensions on EO modulation characteristics.
- The modal overlap factor is systematically examined under different t_{Si} and λ conditions to identify favorable confinement regions for enhanced light–matter interaction.

- A combined framework integrating finite-temperature graphene conductivity modeling, perturbation-based effective-index analysis, and full-wave simulations is employed to investigate the EO behavior of the proposed structure.
- The effects of geometrical variation on effective-index modulation, transmission characteristics, ER, IL, EO bandwidth, and energy-per-bit performance are comprehensively analyzed under different μ_c conditions.
- The obtained results demonstrate that geometry engineering can significantly improve modulation efficiency, propagation characteristics, and EO performance tradeoffs in compact G-PSMs.

Overall, this work establishes a physically interpretable geometry-dependent optimization framework for ultra-thin SOI G-PSMs and provides useful design guidelines for compact broadband EO modulation.

The remainder of this paper is organized as follows. Section 2 presents the proposed G-PSM structure and discusses the operating principles governing modal confinement and EO interaction. Section 3 introduces the theoretical and semi-analytical framework used to model graphene conductivity, modal interaction, and EO performance metrics. Section 4 presents the geometry-dependent performance analysis, including overlap-factor evolution, conductivity behavior, effective-index modulation, transmission characteristics, ER, IL, EO bandwidth, and energy-per-bit performance. Finally, Section 5 summarizes the principal findings of this work.

2. Device Structure and Operating Principle

This section presents the structural configuration and operating mechanism of the proposed G-PSM. First, Section 2.1 describes the hybrid plasmonic slot-waveguide geometry implemented on the ultra-thin SOI platform, including the graphene integration scheme and the principal geometrical parameters governing modal confinement and light–matter interaction. Subsequently, Section 2.2 discusses the EO operating mechanism of the proposed device, with emphasis on the influence of t_{Si} and w_{slot} variation on graphene conductivity interaction and electrically tunable optical behavior. Together, these considerations provide the physical basis for the theoretical framework introduced in Section 3 and the geometry-dependent performance analysis presented later in Section 4.

2.1. Device Geometry

The proposed G-PSM is implemented on a hybrid plasmonic slot-waveguide platform designed to investigate the influence of geometry engineering on optical confinement and EO performance. The structure combines an ultra-thin SOI guiding layer with a nanoscale plasmonic slot region in order to enhance light–matter interaction near the graphene-active layer.

The device operates near the telecommunication wavelength $\lambda = 1550$ nm, where silicon exhibits relatively low optical loss while graphene maintains electrically tunable optical conductivity characteristics [17]. The t_{Si} and w_{slot} are key geometrical parameters governing modal confinement and EO interaction. The graphene layer is electrically biased through the adjacent gold (Au) electrodes forming the plasmonic slot region, enabling dynamic tuning of μ_c. As illustrated in Figure 1, the structure consists of an ultra-thin silicon guiding layer fabricated on a buried oxide (BOX) substrate. Compared with conventional SOI waveguides employing thicker silicon cores, the adopted ultra-thin platform provides stronger confinement control and increased evanescent-field interaction near the graphene-active region.

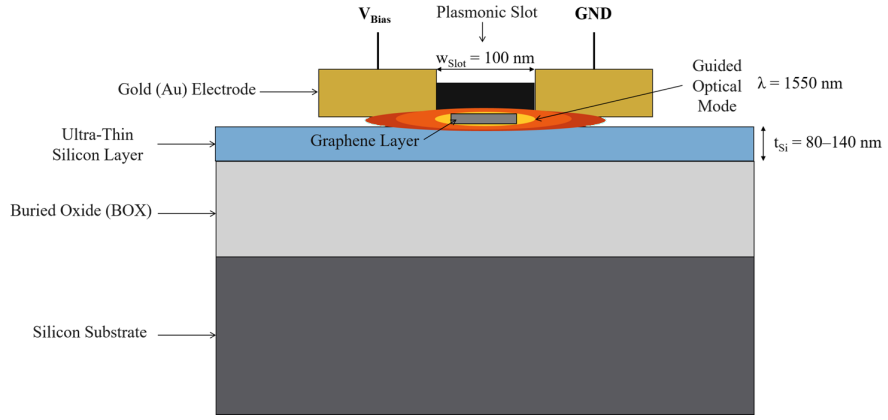


Figure 1. Cross-sectional schematic of the proposed ultra-thin SOI graphene–plasmonic slot modulator (G-PSM), consisting of an ultra-thin silicon guiding layer of thickness t_{Si}, a graphene monolayer embedded within a plasmonic slot of width w_{slot}, Au electrodes, a buried oxide (BOX) layer, and a silicon substrate. The device operates at the telecommunication wavelength $\lambda = 1550$ nm, where strong optical confinement is achieved within the graphene–plasmonic active region.

Metallic electrodes are positioned above the silicon guiding layer and separated by a nanoscale plasmonic slot. Due to the strong electric-field discontinuity at the metal–dielectric interfaces, the optical mode becomes highly compressed inside the slot region [18]. Consequently, strong subwavelength confinement is achieved near the graphene-active layer embedded inside the plasmonic slot.

Au is selected as the plasmonic electrode material owing to its combination of strong plasmonic performance, chemical stability, and extensive use in integrated photonic and graphene-based plasmonic devices operating at telecommunication wavelengths [19]. Although silver can provide lower intrinsic optical losses, its susceptibility to oxidation and material degradation may compromise long-term device stability. Aluminum offers advantages from a CMOS-processing perspective but generally exhibits higher optical losses in the near-infrared spectral region around 1550 nm. Consequently, Au provides a practical compromise between optical performance, fabrication reliability, and device robustness for the proposed G-PSM.

To enhance the EO interaction, a graphene monolayer is integrated directly within the plasmonic slot region, where the optical-field intensity reaches its maximum value [20]. This hybrid configuration significantly increases the modal overlap between the guided optical mode and graphene layer, thereby improving both electro–absorptive and electro–refractive modulation efficiency.

Overall, the proposed geometry-engineered G-PSM establishes the physical basis for the EO investigations presented throughout this work.

2.2. Operating Principle

The operating mechanism of the proposed G-PSM is governed by the interaction between electrically tunable graphene conductivity and the strongly confined hybrid plasmonic mode supported by the ultra-thin SOI structure. By applying an external bias across the graphene layer, μ_c can be dynamically adjusted, thereby modifying the complex optical conductivity of graphene and enabling active control of both optical attenuation and effective-index variation.

At optical frequencies, the graphene conductivity originates from the combined contributions of intraband carrier dynamics and interband electronic transitions [21]. At relatively low μ_c values, interband transitions dominate the optical response, resulting in stronger optical absorption. As μ_c increases, the onset of Pauli blocking suppresses interband absorption and significantly modifies the refractive response of graphene. Consequently,

varying μ_c simultaneously influences both electro–absorptive and electro–refractive modulation behavior.

The plasmonic slot region plays a central role in enhancing the EO interaction strength. The nanoscale slot geometry strongly compresses the electromagnetic field into the low-index region between the metallic electrodes, producing subwavelength confinement and significantly increasing the field intensity near the graphene-active layer. As a result, the overlap between the guided optical mode and graphene becomes substantially enhanced compared with conventional dielectric waveguide configurations.

In addition to graphene conductivity tuning, the proposed G-PSM employs t_{Si} and w_{slot} engineering to control modal confinement and field distribution. Variations in t_{Si} modify the vertical confinement profile and field penetration into the plasmonic slot region, whereas w_{slot} directly affects field localization strength and overlap enhancement. Consequently, the geometrical configuration strongly influences effective-index modulation, transmission characteristics, ER, IL, EO bandwidth, and energy efficiency.

The theoretical framework describing these conductivity-induced modal perturbations is developed in the following section using finite-temperature Kubo conductivity modeling combined with perturbation-based effective-index and overlap-factor analysis.

3. Theoretical Modeling

This section presents the theoretical framework used to analyze the EO behavior of the proposed G-PSM. The formulation combines electrically tunable graphene conductivity with geometry-dependent modal confinement in the ultra-thin SOI platform in order to investigate the influence of μ_c and t_{Si} on effective-index perturbation, transmission behavior, and overall modulation performance.

The developed framework is formulated in a physically interpretable and solver-independent manner to ensure consistency between the semi-analytical model and the numerical eigenmode simulations employed throughout this work. In addition to graphene conductivity modulation, the analysis incorporates overlap-factor evolution and geometry-dependent field redistribution mechanisms governing the interaction between the guided optical mode and the graphene-active region.

Section 3.1 introduces the finite-temperature Kubo formalism used to model the complex optical conductivity of graphene. Section 3.2 then presents the perturbation-based effective-index and overlap-factor analysis used to evaluate conductivity-induced modal variation. Subsequently, Section 3.3 relates the complex effective index to the optical transmission response, while Section 3.4 defines the ER and IL characteristics of the proposed device. Finally, Section 3.5 introduces the energy-per-bit and EO 3 dB bandwidth formulations used to evaluate the speed–energy tradeoff of the proposed G-PSM.

3.1. Graphene Conductivity Model

The EO response of the proposed G-PSM is primarily governed by the electrically tunable complex optical conductivity of graphene. Under external electrostatic biasing, μ_c can be dynamically adjusted, thereby modifying the carrier distribution and altering the interaction between graphene and the confined optical mode. Consequently, conductivity modulation directly influences both the attenuation and phase characteristics of the propagating mode.

At optical frequencies, the graphene conductivity is determined by the combined contributions of intraband carrier transport and interband electronic transitions. Accordingly, the total conductivity is expressed using the finite-temperature Kubo formalism as [22]

$$\sigma(\omega, \mu_c, T_0) = \sigma_{intra}(\omega, \mu_c, T_0) + \sigma_{inter}(\omega, \mu_c, T_0), \quad (1)$$

where ω denotes the optical angular frequency, and T_0 is the operating temperature.

The intraband conductivity originates from free-carrier motion within the same electronic band and is given by [22]

$$\sigma_{\text{intra}} = \frac{2e^2 k_B T_0}{\pi\hbar^2} \frac{i}{\omega + i/\tau} \ln\left[2\cosh\left(\frac{\mu_c}{2k_B T_0}\right)\right], \tag{2}$$

where e is the elementary charge, k_B is Boltzmann's constant, $\hbar$ denotes the reduced Planck constant, and τ is the carrier relaxation time. Increasing μ_c enhances the free-carrier population and therefore strengthens the intraband contribution to the total conductivity.

The interband conductivity component may be expressed as [22]

$$\sigma_{\text{inter}} = \frac{e^2}{4\hbar}\left[\frac{1}{2} + \frac{1}{\pi}\tan^{-1}\left(\frac{\hbar\omega - 2\mu_c}{2k_B T_0}\right) - \frac{i}{2\pi}\ln\left(\frac{(\hbar\omega + 2\mu_c)^2}{(\hbar\omega - 2\mu_c)^2 + (2k_B T_0)^2}\right)\right], \tag{3}$$

where the real part mainly governs optical absorption, while the imaginary part contributes to refractive-index perturbation and phase modulation.

A critical transition occurs when

$$2\mu_c \gtrsim \hbar\omega, \tag{4}$$

corresponding to the onset of Pauli blocking. Under this condition, interband absorption becomes suppressed, resulting in substantial changes in both optical transmission and effective-index modulation.

In the proposed G-PSM, the conductivity-induced EO response is further enhanced by the strong field confinement inside the plasmonic slot region. Since the overlap between the guided optical mode and graphene depends strongly on t_{Si} and slot geometry, conductivity modulation becomes closely coupled to geometry-dependent modal confinement. The finite-temperature Kubo formalism therefore provides a physically consistent framework for analyzing conductivity-induced EO modulation under different geometrical operating conditions.

It should be noted that the graphene conductivity described by the finite-temperature Kubo formalism is inherently temperature dependent. Variations in operating temperature modify the carrier distribution near the Fermi level and therefore produce quantitative changes in both the intraband and interband conductivity components. However, for the moderate temperature fluctuations typically encountered in PICs, the resulting conductivity variation is generally much smaller than the changes induced by electrostatic tuning of μ_c. Consequently, the principal geometry- dependent trends and modulation mechanisms reported in this work are expected to remain stable under normal operating-temperature variations, although the exact values of the effective-index perturbation, transmission, ER, and IL may exhibit minor temperature-dependent shifts.

3.2. Effective-Index Modulation and Modal Overlap

To incorporate the electrically tunable optical response of graphene into the proposed G-PSM, the graphene layer is modeled as an equivalent ultra-thin conductive medium with an effective complex permittivity given by [22]

$$\varepsilon_{g,\text{eff}} = 1 + \frac{i\,\sigma(\omega, \mu_c, T_0)}{\omega\varepsilon_0 t_g}, \tag{5}$$

where ε_0 is the vacuum permittivity and t_g denotes the effective graphene thickness.

The propagation behavior of the guided mode is described by the complex effective index

$$n_{\text{eff}} = n_{\text{eff}}^{(0)} + \Delta n_{\text{eff}}, \tag{6}$$

where Δn_{eff} represents the conductivity-induced modal perturbation. The real and imaginary components of n_{eff} mainly govern phase modulation and propagation attenuation, respectively.

Following the conventional waveguide perturbation framework commonly used for EO and integrated photonic waveguides [23], the effective-index variation may be approximated using first-order perturbation analysis as

$$\Delta n_{\text{eff}} \propto \Gamma \, \Delta\sigma(\omega, \mu_c), \tag{7}$$

where Γ denotes the modal overlap factor and $\Delta\sigma(\omega, \mu_c)$ represents the conductivity variation induced by graphene tuning.

The overlap factor is defined as [24]

$$\Gamma = \frac{\int_{\Omega_g} |E(x,y)|^2 \, dA}{\int_{\Omega_{\text{tot}}} |E(x,y)|^2 \, dA}, \tag{8}$$

where Ω_g represents the graphene-active region and Ω_{tot} denotes the total computational domain.

Accordingly, the overlap factor Γ represents the fraction of the modal electric-field energy interacting with the graphene-active region. It is computed by integrating the normalized electric-field intensity over the graphene interaction region and subsequently normalizing it by the total modal field energy within the computational domain. Larger values of Γ indicate stronger light–matter interaction and greater sensitivity of the guided mode to conductivity variations induced by graphene electrostatic tuning.

In the proposed G-PSM, strong plasmonic confinement substantially enhances the modal overlap near the graphene-active layer. In addition, t_{Si} and slot geometry strongly influence field confinement and penetration into the plasmonic slot region. Consequently, the effective-index perturbation depends on both electrically induced conductivity variation and geometry-dependent modal confinement.

The quantitative values of n_{eff} used throughout this work are extracted using combined eigenmode simulations and semi-analytical calculations.

3.3. Optical Transmission Analysis

The conductivity-induced perturbation in the complex effective index directly influences the transmission characteristics of the proposed G-PSM. Since the imaginary component of n_{eff} governs modal attenuation, the normalized optical transmission through a device of length L may be expressed using the Beer–Lambert relation as [25]

$$T(\mu_c) = \exp\left(-\frac{4\pi}{\lambda} \, \text{Im}(n_{\text{eff}}(\mu_c)) \, L\right), \tag{9}$$

Equation (9) establishes the direct relationship between graphene conductivity tuning and device-level transmission behavior. As μ_c increases and interband absorption becomes progressively suppressed under the Pauli-blocking condition in (4), the imaginary component of n_{eff} decreases, resulting in increased optical transmission.

In the proposed G-PSM, the transmission response is additionally influenced by t_{Si} and slot geometry through their effect on modal confinement and overlap with the

graphene-active region. Stronger field localization enhances the EO interaction but may simultaneously increase propagation loss due to stronger absorption near graphene and the metallic confinement layers. Consequently, the transmission behavior is governed by the coupled interaction between graphene conductivity tuning and geometry-dependent electromagnetic confinement.

3.4. Electro–Optic Performance Metrics

The EO performance of the proposed G-PSM is evaluated using the ER and IL, which characterize the modulation depth and optical attenuation of the device, respectively. The ER and IL are respectively defined as [26]

$$\mathrm{ER} = 10\log_{10}\left(\frac{T_{\mathrm{ON}}}{T_{\mathrm{OFF}}}\right), \tag{10}$$

$$\mathrm{IL} = -10\log_{10}(T_{\mathrm{ON}}), \tag{11}$$

where T_{ON} and T_{OFF} denote the transmitted optical powers corresponding to the ON and OFF states, respectively.

Both ER and IL are evaluated directly from (9). Since the transmission response depends strongly on modal confinement and overlap with the graphene-active region, both metrics are influenced by t_{Si} and slot geometry. Stronger confinement generally enhances the EO interaction but may simultaneously increase propagation attenuation due to stronger absorption near graphene and the metallic confinement layers.

3.5. Energy Consumption and Bandwidth Metrics

In addition to ER and IL, the practical performance of the proposed G-PSM is governed by the tradeoff between switching energy and modulation bandwidth. The energy consumed per transmitted bit is approximated by

$$E_{\mathrm{bit}} = \frac{1}{4}CV_{\mathrm{drive}}^2, \tag{12}$$

where C is the effective device capacitance and V_{drive} denotes the applied driving voltage.

The EO 3 dB bandwidth is approximated using the RC-limited response

$$f_{3\mathrm{dB}} = \frac{1}{2\pi RC}, \tag{13}$$

where R and C represent the effective resistance and capacitance, respectively. The 3-dB EO bandwidth is estimated using the conventional RC-limited small-signal response model, in which the modulation speed is primarily determined by the electrical charging and discharging dynamics of the active device region. This approximation is widely adopted for graphene-based EO modulators and assumes that other potential limitations, including carrier transit time and intrinsic graphene carrier-response dynamics, remain negligible compared with the RC delay under the investigated operating conditions. In particular, graphene exhibits ultrafast carrier dynamics on sub-picosecond timescales, corresponding to intrinsic response frequencies well beyond the hundreds-of-gigahertz range considered in this study. Therefore, the overall EO bandwidth of the proposed G-PSM is primarily governed by the effective device resistance and capacitance rather than by intrinsic material-speed limitations.

In the proposed G-PSM, t_{Si} and slot geometry strongly influence both field confinement and capacitance inside the plasmonic slot region. Narrower slots generally enhance modal overlap and EO interaction while reducing the active device volume, thereby improving bandwidth performance and lowering the energy-per-bit consump-

tion. Equations (12) and (13) therefore establish the theoretical basis for evaluating the speed–energy tradeoff investigated in Section 4.5.

The theoretical framework developed throughout this section establishes a direct physical relationship between graphene conductivity tuning, geometry-dependent modal confinement, effective-index modulation, optical transmission behavior, and device-level EO performance metrics, including ER, IL, energy-per-bit consumption, and EO bandwidth. Furthermore, the proposed framework remains fully compatible with eigenmode simulations, full-wave electromagnetic analysis, and MATLAB R2025b parametric investigations, thereby enabling physically consistent interpretation of the geometry-dependent numerical results presented in Section 4.

It should be noted that both the graphene relaxation time and operating temperature influence the Kubo conductivity and, consequently, the EO response of graphene-based devices. However, the primary objective of the present study is to investigate geometry-dependent performance optimization under a common set of operating conditions. Accordingly, all simulations were performed at $T_0 = 300$ K and $\tau = 100$ fs. Although variations in these parameters may lead to quantitative changes in conductivity and modulation strength, the relative trends associated with t_{Si} and plasmonic-slot engineering are expected to remain qualitatively unchanged.

4. Results and Discussion

This section presents the numerical investigation and EO performance analysis of the proposed thickness-engineered hybrid G-PSM using a combined framework consisting of eigenmode simulations, full-wave three-dimensional finite-difference time-domain (3D-FDTD) analysis, and semi-analytical MATLAB R2025b modeling. Particular emphasis is placed on evaluating the influence of μ_c and t_{Si} variation on modal confinement, overlap-factor evolution, effective-index perturbation, and device-level EO modulation characteristics.

The discussion is organized according to the principal physical mechanisms governing the operation of the proposed structure. Section 4.1 first examines the electromagnetic field distribution and modal confinement characteristics of the supported hybrid plasmonic mode. Subsequently, Section 4.2 investigates the thickness-dependent evolution of the overlap factor between the guided optical mode and the graphene-active region in order to identify the geometrical conditions that maximize light–matter interaction.

Next, Section 4.3 investigates the influence of t_{Si} engineering on the effective refractive-index perturbation induced by graphene conductivity modulation. The device-level EO response is subsequently evaluated in Section 4.4 through detailed analysis of the optical transmission, ER, and IL characteristics as functions of μ_c and t_{Si}. Section 4.5 investigates the energy-per-bit consumption and 3 dB EO bandwidth characteristics of the proposed G-PSM in order to evaluate the speed–energy tradeoff under different t_{Si} conditions. Finally, Section 4.6 compares the obtained performance metrics with representative graphene-based and graphene–plasmonic modulators reported in the literature, thereby placing the proposed G-PSM within the context of the current state of the art and highlighting its overall performance tradeoffs and design advantages.

Unless otherwise specified, all simulations were performed at room temperature ($T_0 = 300$ K) using the baseline hybrid graphene–plasmonic structure introduced previously in Section 2. The optical conductivity of graphene was modeled using the finite-temperature Kubo formalism. Unless otherwise stated, the graphene relaxation time is assumed to be $\tau = 100$ fs, which is a commonly adopted value in the literature for near-infrared graphene-based EO devices and provides a realistic representation of carrier scattering effects under practical operating conditions [3]. In the numerical simulations, local mesh refinement was employed near the graphene and plasmonic slot regions to

accurately resolve the strongly confined electromagnetic fields, while perfectly matched layer (PML) boundary conditions were applied to minimize artificial reflections at the simulation boundaries.

The baseline device operates near the telecommunication wavelength $\lambda = 1550$ nm and consists of an ultra-thin silicon guiding layer with width $w_{\mathrm{Si}} = 800$ nm positioned on a buried oxide (BOX) substrate with thickness $t_{\mathrm{BOX}} = 1000$ nm. The plasmonic region comprises two Au electrodes with width $w_{\mathrm{Au}} = 250$ nm and height $h_{\mathrm{Au}} = 120$ nm separated by a nanoscale slot with width $w_{\mathrm{slot}} = 100$ nm. A graphene monolayer with effective thickness $t_g = 0.34$ nm is embedded inside the slot region, while the structure is covered by a top cladding layer with thickness $t_{\mathrm{clad}} = 800$ nm. The t_{Si} is systematically varied throughout this work in order to investigate its influence on optical confinement, modal overlap, effective-index perturbation, transmission characteristics, ER, and IL within the proposed hybrid G-PSM.

For the full-wave analysis, 3D-FDTD simulations employed guided-mode excitation together with optical power monitors to evaluate the transmission response, effective-index perturbation, ER, IL, and propagation attenuation under different μ_c and t_{Si} conditions. The investigated μ_c range extends from 0 eV to 1 eV, while the t_{Si} was varied over representative ultra-thin SOI dimensions in order to analyze the relationship between geometrical confinement and EO performance optimization.

4.1. Eigenmode Analysis

The electromagnetic characteristics of the proposed G-PSM were investigated using the finite-difference eigenmode (FDE) solver in Lumerical 2026 R1 MODE at $\lambda = 1550$ nm. The graphene optical response was incorporated using the finite-temperature Kubo conductivity model together with the equivalent thin-film permittivity formulation presented in Section 3.

To accurately resolve the strongly confined fields near the plasmonic slot interfaces, local mesh refinement was applied near the graphene layer and metallic boundaries, while PMLs were employed to suppress artificial reflections.

The analysis focuses on the fundamental hybrid plasmonic mode supported by the proposed structure. The extracted mode exhibits quasi-TM characteristics with strong transverse electric-field confinement inside the plasmonic slot region. The eigenmode solver simultaneously provides the complex effective refractive index required for evaluating both phase propagation and modal attenuation characteristics.

Figure 2 illustrates the spatial distribution of the dominant electric-field component E_x. Strong electromagnetic localization is clearly observed inside the nanoscale plasmonic slot near graphene, confirming efficient subwavelength confinement and enhanced concentration of optical energy inside the active modulation region.

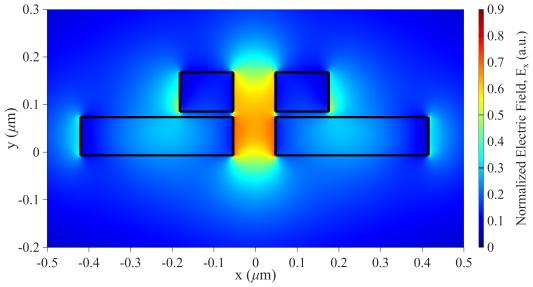


Figure 2. Spatial distribution of the normalized dominant transverse electric-field component E_x for the fundamental hybrid mode at $\lambda = 1550$ nm. The field distribution is normalized to its maximum value, and the color scale represents relative field intensity (a.u.). Strong optical confinement is observed inside the plasmonic slot region near the graphene layer, demonstrating enhanced electromagnetic localization and efficient light–matter interaction.

The obtained mode profile further demonstrates the hybrid plasmonic–photonic nature of the proposed structure, in which the optical energy is simultaneously distributed between the ultra-thin silicon guiding layer and the nanoscale plasmonic slot region adjacent to graphene. Strong optical confinement is maintained inside the nanoscale plasmonic slot, while a significant fraction of the optical energy remains distributed within the adjacent ultra-thin silicon layer. As the t_{Si} decreases, the optical confinement provided by the silicon guiding layer is weakened, allowing a larger fraction of the electromagnetic field to penetrate into the plasmonic slot and graphene-active region. Consequently, the modal overlap with graphene increases, resulting in stronger light–matter interaction and enhanced EO modulation efficiency. Conversely, increasing the t_{Si} promotes stronger confinement within the silicon region and reduces the field fraction residing in the plasmonic slot, thereby decreasing the overlap factor and the strength of the EO interaction. These observations provide physical insight into the t_{Si}-dependent behavior reported in the following sections.

4.2. Modal Overlap Analysis

The overlap factor Γ is strongly influenced not only by the geometrical confinement of the proposed G-PSM, but also by λ through its effect on modal distribution and plasmonic field localization. Consequently, investigating the wavelength dependence of Γ is essential for evaluating the broadband EO behavior of the proposed structure and identifying favorable operating conditions for efficient light–matter interaction.

Figure 3 illustrates the variation of the overlap factor Γ as a function of t_{Si} for operating wavelengths of 1490 nm, 1550 nm, and 1625 nm. All investigated wavelengths exhibit a distinct non-monotonic dependence on t_{Si}, with Γ varying approximately between 0.0415 and 0.0448.

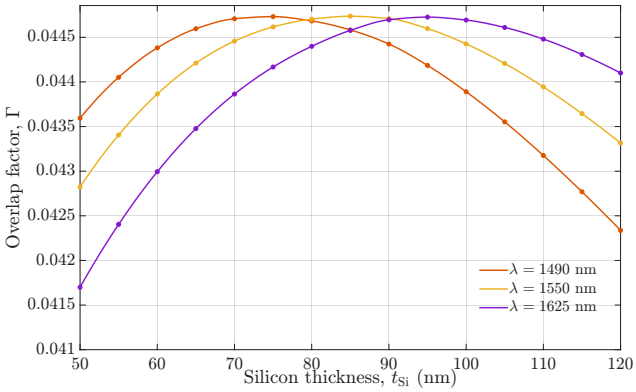


Figure 3. Overlap factor Γ as a function of silicon thickness t_{Si} for representative telecommunication wavelengths. Markers represent values extracted from Lumerical 2026 R1 simulations, while solid lines illustrate the corresponding trend evolution.

This behavior originates from the balance between dielectric confinement inside the ultra-thin SOI layer and plasmonic field localization within the slot region. For very small t_{Si}, the optical mode becomes weakly confined and a portion of the field extends away from the graphene-active region, limiting the achievable overlap. As t_{Si} increases, stronger field localization near the plasmonic slot enhances the interaction between the guided mode and graphene, resulting in an increase in Γ. Beyond the optimum thickness region, however, additional confinement within the silicon layer reduces the fraction of optical energy residing in the plasmonic slot and graphene-active region, causing the overlap factor to decrease. This behavior is consistent with the hybrid mode profile shown in Figure 2 and demonstrates that t_{Si} engineering provides an effective mechanism for maximizing light–matter interaction in the proposed G-PSM.

For relatively thin silicon layers near $t_{Si} = 50$ nm, the overlap factor remains comparatively low due to weak vertical confinement, allowing a significant portion of the optical field to spread into the surrounding dielectric regions. Quantitatively, the overlap factor is approximately $\Gamma \approx 0.0436$, $\Gamma \approx 0.0428$, and $\Gamma \approx 0.0417$ for operating wavelengths of 1490 nm, 1550 nm, and 1625 nm, respectively. Under these conditions, the shorter wavelength exhibits stronger confinement near the graphene-active region.

As t_{Si} increases, stronger dielectric confinement gradually drives the optical field toward the plasmonic slot region, thereby enhancing the overlap with graphene. All investigated wavelengths exhibit progressive improvement in Γ until reaching maximum values near $t_{Si} \approx 75$–100 nm. The highest overlap is obtained near $\lambda = 1550$ nm and $t_{Si} \approx 85$ nm, where Γ reaches approximately 0.0447. In comparison, the peak overlap for $\lambda = 1490$ nm occurs near $t_{Si} \approx 75$ nm, while the longest wavelength of 1625 nm reaches its maximum near $t_{Si} \approx 95$ nm. Physically, longer wavelengths exhibit broader modal distributions and therefore require slightly stronger dielectric confinement to maximize field localization near graphene.

Beyond the optimum thickness region, the overlap factor gradually decreases for all wavelengths as the optical mode becomes increasingly confined inside the silicon core rather than within the plasmonic slot region. At $t_{Si} = 120$ nm, the overlap factor decreases to approximately $\Gamma \approx 0.0423$, $\Gamma \approx 0.0433$, and $\Gamma \approx 0.0441$ for wavelengths of 1490 nm, 1550 nm, and 1625 nm, respectively.

Overall, the results demonstrate that the overlap factor is governed by the coupled influence of wavelength-dependent modal confinement and t_{Si} engineering. The identified optimum region therefore provides a physically balanced operating condition capable of maximizing light–matter interaction while maintaining stable broadband EO performance.

4.3. Effective-Index Modulation

Electrically induced effective-index modulation represents one of the principal EO operating mechanisms of the proposed G-PSM. Variations in graphene conductivity modify the propagation constant of the guided optical mode, resulting in a perturbation of the complex effective index. Consequently, the evolution of Δn_{eff} with μ_c provides direct insight into the EO response of the device and its phase- and absorption-modulation capabilities.

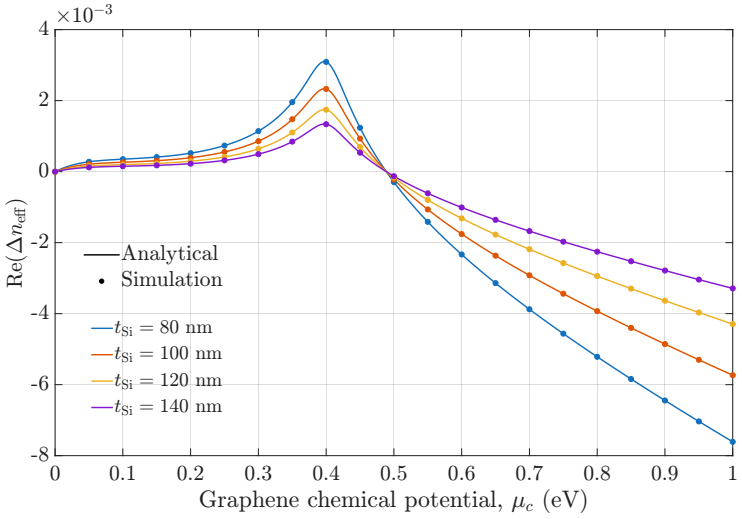
For clarity, the complex effective-index perturbation is decomposed into its real and imaginary components. The real part, $\mathrm{Re}(\Delta n_{eff})$, is associated with phase modulation through changes in the propagation constant of the guided mode, whereas the imaginary part, $\mathrm{Im}(\Delta n_{eff})$, governs optical attenuation and therefore directly determines absorption-based modulation behavior.

Figure 4a illustrates the variation of the real part of the effective-index perturbation, $\mathrm{Re}(\Delta n_{eff})$, as a function of μ_c for different t_{Si} ranging from 80 nm to 140 nm, while Figure 4b presents the corresponding imaginary component, $\mathrm{Im}(\Delta n_{eff})$.

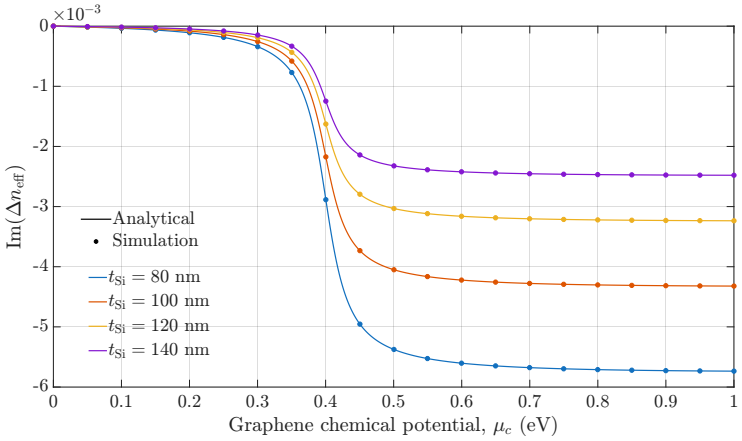
Excellent agreement is observed between the semi-analytical and numerical results over the entire investigated μ_c range, confirming the validity of the conductivity-driven perturbation model adopted for the proposed G-PSM.

The real part of the effective-index perturbation exhibits a pronounced non-monotonic dependence on μ_c for all investigated values of t_{Si}. At relatively low chemical potentials ($\mu_c \lesssim 0.2$ eV), the induced refractive-index variation remains small and close to zero, indicating a limited perturbation of the guided optical mode. As μ_c increases, $\mathrm{Re}(\Delta n_{eff})$ rises progressively and reaches its maximum value near $\mu_c \approx 0.4$ eV. Quantitatively, the peak effective-index perturbation reaches approximately 3.1×10^{-3} for $t_{Si} = 80$ nm and decreases gradually to approximately 1.3×10^{-3} for $t_{Si} = 140$ nm. Intermediate thicknesses of 100 nm and 120 nm produce peak values of approximately 2.3×10^{-3} and

1.8×10^{-3}, respectively. These results indicate that thinner silicon layers provide stronger modal interaction with graphene and therefore larger conductivity-induced refractive-index perturbations.



(**a**)



(**b**)

Figure 4. Variation of the complex effective-index perturbation as a function of graphene chemical potential μ_c for different silicon thicknesses: (**a**) real part of the effective-index change, $\mathrm{Re}(\Delta n_{\mathrm{eff}})$, governing electro–refractive (phase) modulation, and (**b**) imaginary part of the effective-index change, $\mathrm{Im}(\Delta n_{\mathrm{eff}})$, governing electro–absorptive modulation and propagation attenuation. Solid lines represent semi-analytical results, while markers correspond to numerical simulation data.

For the operating wavelength of $\lambda = 1550$ nm, the photon energy is approximately $\hbar\omega \approx 0.8$ eV. Consequently, the Pauli-blocking condition $2\mu_c \approx \hbar\omega$ is satisfied near $\mu_c \approx 0.4$ eV. Below this threshold, interband electronic transitions dominate the graphene optical response. As the μ_c approaches and exceeds this value, interband absorption becomes progressively suppressed while intraband carrier dynamics become increasingly important. This conductivity transition modifies both the dispersive and absorptive components of the graphene response and therefore strongly influences the effective-index perturbation.

Beyond the transition region, $\mathrm{Re}(\Delta n_{\mathrm{eff}})$ gradually decreases and eventually becomes negative at larger μ_c. At $\mu_c \approx 1$ eV, the effective-index perturbation reaches approximately -7.6×10^{-3} for $t_{\mathrm{Si}} = 80$ nm and approximately -3.3×10^{-3} for $t_{\mathrm{Si}} = 140$ nm. This sign reversal reflects a change in the dominant dispersive mechanism governing the graphene optical response.

The observed sign reversal of Δn_{eff} originates from the conductivity transition occurring near the Pauli-blocking threshold. Below this threshold, interband electronic transitions dominate the graphene optical response and produce a positive conductivity-induced perturbation of the effective refractive index. As μ_c approaches and exceeds the Pauli-blocking condition, interband absorption becomes progressively suppressed while the intraband contribution increases. Consequently, the imaginary component of the graphene conductivity undergoes a transition in its dominant dispersive behavior, causing Δn_{eff} to reach a maximum near $\mu_c \approx 0.4$ eV and subsequently change sign. Physically, this reflects a transition from interband-dominated to intraband-dominated carrier dynamics, resulting in the observed reversal of the effective-index perturbation of the hybrid plasmonic mode.

Figure 4b provides the corresponding variation of the imaginary component of the effective-index perturbation, $\text{Im}(\Delta n_{\text{eff}})$, which governs modal attenuation and absorption-based modulation. Excellent agreement is again observed between the semi-analytical predictions and numerical simulations, confirming the validity of the developed conductivity-driven model for describing attenuation perturbations in the proposed G-PSM.

Unlike the real component, which exhibits a peak followed by a sign reversal, the imaginary component decreases monotonically as the μ_c increases. For all investigated values of t_{Si}, $\text{Im}(\Delta n_{\text{eff}})$ remains close to zero at low μ_c and then undergoes a sharp transition within the range $\mu_c \approx 0.35$–0.45 eV. This transition coincides with the onset of Pauli blocking, where interband electronic transitions become progressively suppressed, producing a substantial reduction in graphene absorption.

Quantitatively, at $\mu_c = 1$ eV, the attenuation perturbation reaches approximately -5.8×10^{-3}, -4.3×10^{-3}, -3.2×10^{-3}, and -2.5×10^{-3} for t_{Si} of 80 nm, 100 nm, 120 nm, and 140 nm, respectively. The magnitude of $\text{Im}(\Delta n_{\text{eff}})$ therefore decreases systematically with increasing t_{Si}, indicating weaker attenuation modulation for thicker silicon guiding layers.

The observed thickness dependence originates from the geometry-controlled modal confinement characteristics of the proposed structure. Thinner silicon layers allow a larger fraction of the optical field to penetrate into the graphene-loaded plasmonic slot region, thereby strengthening light–matter interaction and increasing the conductivity-induced attenuation perturbation. Conversely, increasing the t_{Si} confines a greater portion of the optical energy within the dielectric core, reducing overlap with graphene and consequently decreasing the magnitude of $\text{Im}(\Delta n_{\text{eff}})$. This behavior is fully consistent with the overlap-factor trends presented in Figure 3 and confirms that geometry-dependent modal confinement strongly influences absorption-based EO modulation.

The evolution of the real and imaginary components of the effective index directly influences the device-level EO performance. Variations in $\text{Re}(\Delta n_{\text{eff}})$ determine the strength of phase modulation, whereas variations in $\text{Im}(\Delta n_{\text{eff}})$ govern modal attenuation and are therefore directly reflected in the transmission, ER, and IL characteristics presented in Section 4.4.

Overall, the results demonstrate that the effective-index modulation characteristics of the proposed G-PSM are governed by the combined effects of graphene conductivity tuning and geometry-dependent modal confinement. The transition region near $\mu_c \approx 0.35$–0.45 eV represents a favorable operating regime in which strong conductivity-induced perturbations are obtained while maintaining efficient light–matter interaction and compact device dimensions. The excellent agreement between the semi-analytical framework and numerical simulations further validates the proposed methodology for predicting geometry-dependent EO performance in ultra-thin SOI G-PSMs.

4.4. Electro–Optic Performance Analysis

The EO performance of the proposed G-PSM is strongly governed by the coupled interaction between graphene conductivity tuning and geometry-dependent modal confinement. Since variations in t_{Si} directly modify the overlap between the guided optical mode and the graphene-active region, analyzing the simultaneous evolution of T, ER, and IL as functions of t_{Si} and μ_c provides important insight into the optimum operating conditions of the proposed structure. Therefore, two-dimensional EO performance maps are investigated over t_{Si} ranging from 80 nm to 140 nm and μ_c extending from 0 eV to 1 eV.

Figure 5a presents the two-dimensional optical-transmission map of the proposed G-PSM as functions of t_{Si} and μ_c. The contour lines correspond to constant transmission levels and provide direct visualization of the geometry-dependent EO transmission behavior.

A pronounced nonlinear transition boundary separating high-transmission and low-transmission operating regions is clearly observed across the (t_{Si}, μ_c) plane. At relatively small μ_c below approximately $\mu_c \approx 0.35$ eV, the transmission remains comparatively low, with values typically ranging between approximately $T \approx 0.35$ and 0.45 depending on t_{Si}. In this regime, interband transitions dominate the graphene optical response, producing comparatively strong modal attenuation inside the plasmonic slot region.

As μ_c increases toward the transition region near $\mu_c \approx 0.4$ eV, the transmission rises rapidly due to the onset of Pauli blocking and the resulting suppression of interband absorption. The contour distribution reveals a steep transition from low-transmission to high-transmission operation over a relatively narrow μ_c interval. Beyond this region, the transmission gradually approaches values exceeding approximately $T \approx 0.9$ for thinner silicon layers near $t_{Si} = 80$ nm.

The influence of t_{Si} is also physically significant. Increasing t_{Si} systematically reduces the transmission throughout the investigated operating range. For example, at $\mu_c \approx 1$ eV, the transmission decreases from approximately $T \approx 0.95$ for $t_{Si} = 80$ nm to nearly $T \approx 0.65$ for $t_{Si} = 140$ nm. This behavior originates from the thickness-dependent redistribution of optical energy between the dielectric guiding region and the plasmonic slot region, which directly modifies the interaction strength with graphene.

Figure 5b illustrates the corresponding ER map of the proposed G-PSM as functions of t_{Si} and μ_c. The contour lines represent constant ER levels and demonstrate the electrically tunable modulation contrast achieved under different geometrical conditions.

At comparatively low chemical potentials below approximately $\mu_c \approx 0.35$ eV, the ER remains relatively weak, typically below approximately 0.5 dB for all investigated t_{Si} values. In this operating regime, the conductivity-induced perturbation imposed on the guided optical mode remains comparatively limited, resulting in relatively small transmission differences between the modulation states.

As μ_c increases beyond the transition region near approximately 0.4 eV, the ER rises sharply due to the strong conductivity-dependent modification of the hybrid plasmonic mode. Quantitatively, the ER reaches values approaching approximately 3.5 dB for thinner silicon layers near $t_{Si} = 80$ nm and high chemical potentials close to $\mu_c = 1$ eV. In contrast, increasing the t_{Si} gradually reduces the achievable ER, with values decreasing toward approximately 1.5 dB for $t_{Si} = 140$ nm.

The compressed contour spacing observed near the transition region indicates strong EO sensitivity, where relatively small variations in μ_c produce substantial modulation-depth changes. Physically, thinner silicon layers enhance modal overlap and field penetration into the plasmonic slot region, thereby strengthening the interaction between the guided optical mode and graphene and consequently improving the achievable modulation contrast.

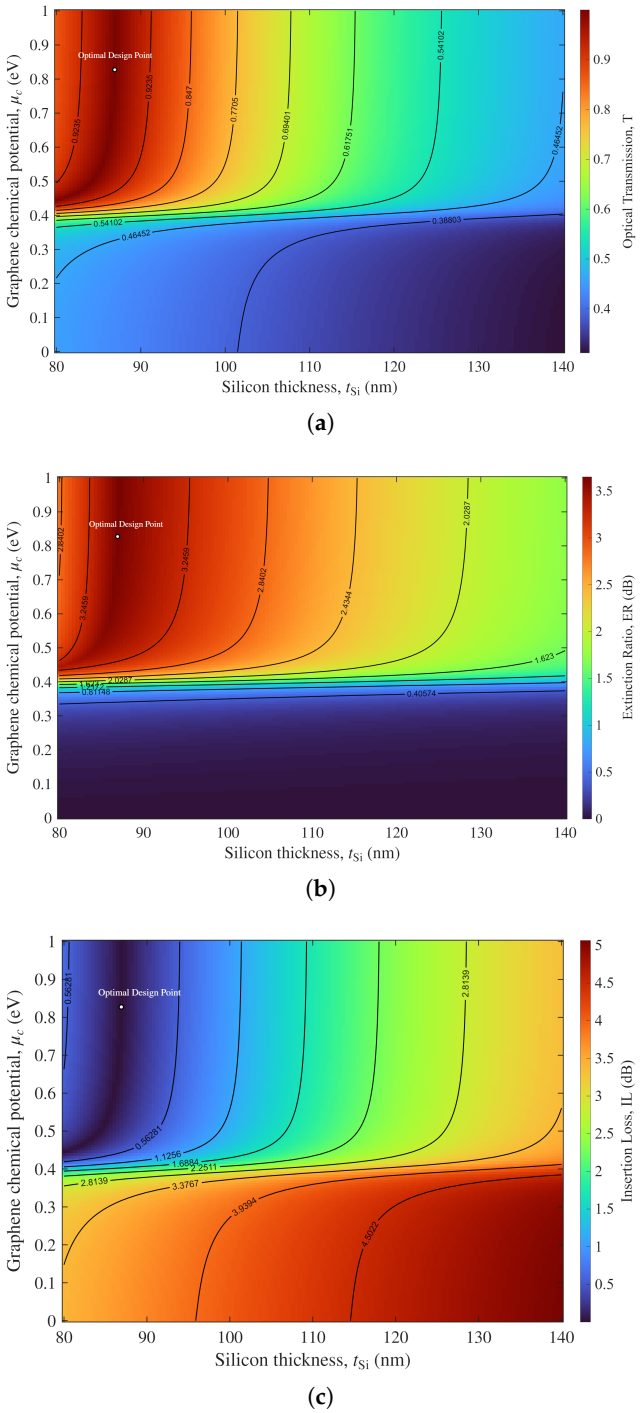


Figure 5. Two-dimensional EO performance maps of the proposed G-PSM as functions of silicon thickness t_{Si} and graphene chemical potential μ_c: (**a**) optical transmission T, (**b**) extinction ratio ER, and (**c**) insertion loss IL. The contour lines represent constant performance levels and illustrate the coupled influence of geometry-dependent modal confinement and graphene conductivity tuning on the EO response.The circular marker indicates the optimum operating point corresponding to the most favorable ER/IL tradeoff.

Figure 5c presents the IL characteristics of the proposed G-PSM as functions of t_{Si} and μ_c. The contour map provides direct insight into the geometry-dependent propagation attenuation experienced by the guided optical mode under different electrical operating conditions.

A pronounced nonlinear transition boundary is clearly observed near $\mu_c \approx 0.4$ eV across the (t_{Si}, μ_c) plane. At relatively low μ_c below this transition region, the IL remains

comparatively large, particularly for thicker silicon layers, with values approaching approximately 3–5 dB. In this regime, strong interband absorption in graphene increases the attenuation experienced by the guided hybrid mode inside the plasmonic slot region.

As the μ_c increases beyond the transition region, the IL decreases progressively due to the onset of Pauli blocking and the resulting suppression of interband absorption. Quantitatively, the IL decreases toward approximately 1.5–2 dB for thinner silicon layers near $t_{Si} = 80$ nm at high μ_c close to $\mu_c = 1$ eV.

The influence of t_{Si} is also physically significant. Increasing t_{Si} systematically increases the IL throughout the investigated operating range. Thicker silicon layers modify the modal field distribution and increase the effective propagation attenuation experienced by the hybrid optical mode. In contrast, thinner silicon layers maintain comparatively lower attenuation while preserving efficient EO interaction inside the plasmonic slot region.

The compressed contour spacing observed near the transition boundary further indicates strong EO sensitivity, where relatively small variations in μ_c produce substantial changes in modal attenuation. Physically, this behavior originates from the strong conductivity-dependent perturbation imposed on the hybrid plasmonic mode near the transition between interband-dominated and Pauli-blocked operating regimes.

Overall, the obtained results demonstrate that the IL characteristics of the proposed G-PSM are strongly governed by the coupled interaction between graphene conductivity tuning and geometry-dependent modal confinement. The identified operating region near $\mu_c \approx 0.4$ eV together with relatively thin silicon layers therefore provides a physically balanced condition capable of maintaining moderate propagation loss while preserving efficient EO modulation performance.

To provide a clearer design guideline, the optimum operating point identified from the two-dimensional performance maps is highlighted in Figure 5. The selected design point corresponds to $t_{Si} \approx 87$ nm and $\mu_c \approx 0.83$ eV, where the proposed G-PSM achieves a favorable balance between a high ER and a relatively low IL. This operating condition therefore represents a practical tradeoff between modulation efficiency and propagation performance, providing useful design guidance for the implementation of geometry-engineered graphene–plasmonic EO modulators.

4.5. Energy-per-Bit and Bandwidth Analysis

In addition to ER, IL, and effective-index tunability, the practical performance of compact EO modulators is strongly governed by the tradeoff between switching energy and modulation bandwidth. Consequently, evaluating the evolution of the energy-per-bit consumption E_{bit} and the corresponding 3 dB EO bandwidth f_{3dB} is essential for assessing the suitability of the proposed G-PSM for low-power high-speed integrated photonic systems.

Figure 6 illustrates the variation of E_{bit} and f_{3dB} as functions of the μ_c for t_{Si} ranging from $t_{Si} = 80$ nm to 140 nm. Curves represent the semi-analytical model, while circular markers correspond to numerical simulation results. Strong agreement is observed between the analytical and numerical data throughout the investigated μ_c range, confirming the consistency of the adopted EO performance framework.

A pronounced inverse relationship between energy consumption and modulation bandwidth is observed for all investigated t_{Si} values. At relatively low μ_c below approximately $\mu_c \approx 0.25$ eV, the energy-per-bit remains comparatively high while the achievable EO bandwidth is limited. Quantitatively, the structure with $t_{Si} = 80$ nm exhibits an initial energy consumption near approximately 14 fJ/bit together with a bandwidth close to approximately 80 GHz. Increasing the silicon thickness to $t_{Si} = 140$ nm further increases the

energy consumption toward approximately 17.5 fJ/bit while reducing the corresponding bandwidth toward nearly 70 GHz.

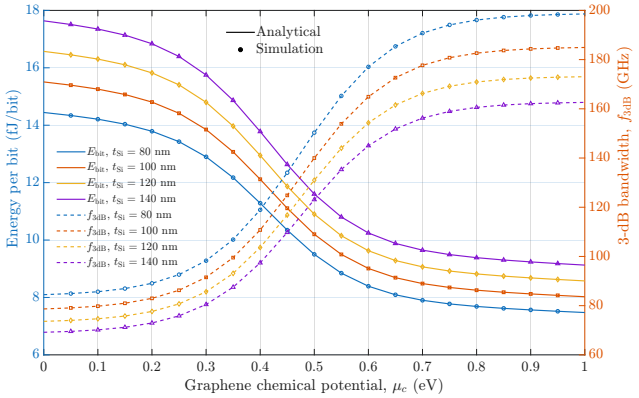


Figure 6. Energy-per-bit consumption E_{bit} and 3 dB EO bandwidth f_{3dB} as functions of graphene chemical potential μ_c for different silicon thicknesses. Solid lines represent semi-analytical results, while circular markers denote numerical simulation data.

As the μ_c increases, the energy-per-bit decreases progressively while the EO bandwidth simultaneously increases. The strongest transition occurs within the approximate range $\mu_c \approx 0.35$–0.6 eV, where the conductivity evolution of graphene produces substantial modification of the RC-limited EO response. Within this transition region, the suppression of interband absorption together with the increasing influence of intraband carrier dynamics improves the electrically induced modulation efficiency and enhances the achievable bandwidth performance.

At larger chemical potentials approaching $\mu_c \approx 1$ eV, the proposed G-PSM exhibits substantially improved speed–energy characteristics. Quantitatively, the structure with $t_{Si} = 80$ nm achieves the best overall performance, where the energy-per-bit decreases toward approximately 7.5 fJ/bit while the corresponding EO bandwidth approaches nearly 200 GHz. In contrast, increasing the silicon thickness to $t_{Si} = 140$ nm produces comparatively larger energy consumption near approximately 9 fJ/bit together with reduced bandwidth values approaching approximately 165 GHz. Intermediate thicknesses of 100 nm and 120 nm exhibit performance trends between these two operating extremes.

From a physical perspective, thinner silicon layers enhance modal overlap and strengthen electromagnetic confinement near the graphene-active region, thereby improving the efficiency of conductivity-induced EO modulation. Stronger confinement simultaneously reduces the effective active volume and capacitive loading, leading to lower switching energy and faster EO response. In contrast, thicker silicon layers confine a larger fraction of the optical field inside the dielectric guiding region, reducing the interaction strength with graphene and consequently degrading the achievable speed–energy performance.

Overall, the obtained results confirm that the proposed ultra-thin SOI-assisted G-PSM simultaneously supports low-energy operation and high-speed EO modulation within a compact integrated photonic platform. The coexistence of reduced switching energy and enhanced bandwidth near the conductivity-transition region further demonstrates the effectiveness of geometry-dependent confinement engineering for future low-power high-speed PICs.

From a fabrication perspective, the proposed G-PSM is expected to exhibit reasonable robustness against typical dimensional variations encountered in advanced silicon-photonics manufacturing processes. Since the EO performance varies smoothly with t_{Si} over most of the investigated parameter range, small fabrication deviations are expected to produce only gradual changes in modal confinement, overlap factor, and effective-index

perturbation. Consequently, moderate variations in t_{Si} would primarily lead to quantitative shifts in transmission, ER, and IL rather than altering the overall performance trends identified in this work. A comprehensive tolerance and statistical-yield analysis constitutes an interesting topic for future investigation.

From a practical perspective, the predicted performance metrics compare favorably with those reported for contemporary graphene-based EO modulators. In particular, the combination of approximately 7.5 fJ/bit energy consumption and a 3 dB bandwidth approaching 200 GHz demonstrates the potential of the proposed architecture for high-speed and energy-efficient PICs, optical interconnects, and next-generation on-chip optical communication systems.

4.6. Comparison with Previously Reported Graphene-Based Modulators

To further assess the performance of the proposed G-PSM, Table 1 compares its key EO characteristics with representative graphene-based and graphene–plasmonic modulators reported in the literature. The comparison includes ER, IL, energy-per-bit consumption, and modulation bandwidth, which are among the most important figures of merit for evaluating practical integrated EO modulators.

Table 1. Performance comparison with representative graphene-based modulators.

Work	ER (dB)	IL (dB)	Energy/bit (fJ/bit)	Bandwidth (GHz)
[27]	15.95	1.89	N/R	N/R
[28]	3.5	6.2	242	N/R
This Work	16.4	2.0	7.5	200

As shown in Table 1, the proposed G-PSM achieves an ER of 16.4 dB with an IL of approximately 2 dB, which is comparable to or better than several previously reported graphene-based plasmonic modulators. In addition, the proposed structure exhibits an estimated energy consumption of 7.5 fJ/bit together with a 3 dB EO bandwidth approaching 200 GHz, indicating its suitability for high-speed and energy-efficient optical interconnect applications.

While some previously reported devices demonstrate advantages in specific performance metrics, the proposed G-PSM provides a balanced combination of strong modulation depth, low IL, high-speed operation, and compact device implementation. More importantly, unlike many earlier studies that primarily focused on demonstrating device performance under fixed geometrical configurations, the present work systematically investigates the influence of ultra-thin t_{Si} engineering on modal confinement, overlap enhancement, effective-index perturbation, transmission characteristics, energy consumption, and bandwidth performance. This geometry-dependent optimization framework provides additional physical insight into the design of G-PSMs and offers practical guidelines for achieving improved EO performance in future integrated photonic platforms.

5. Conclusions

An ultra-thin SOI G-PSM has been proposed and investigated using a combined semi-analytical and numerical framework. By integrating graphene inside a strongly confined plasmonic slot region, the proposed architecture achieves enhanced light–matter interaction together with efficient EO modulation in a compact integrated photonic platform.

The obtained results demonstrate that geometry engineering through t_{Si} optimization strongly influences modal confinement, overlap enhancement, effective-index perturbation, transmission characteristics, ER, IL, energy-per-bit consumption, and EO bandwidth.

Strong electromagnetic localization near the graphene-active region enables efficient electro–absorptive and electro–refractive modulation under compact device dimensions.

The proposed G-PSM exhibits pronounced EO tunability near the conductivity-transition region associated with the onset of Pauli blocking. Quantitatively, the structure achieves effective refractive-index variations approaching approximately 3.1×10^{-3}, transmission values exceeding approximately 0.9, ER values near approximately 3.5 dB, and IL values around approximately 1.5–2 dB under optimized operating conditions.

The speed–energy analysis further confirms the suitability of the proposed architecture for low-power high-speed photonic systems. The optimized structure achieves energy-per-bit consumption approaching approximately 7.5 fJ/bit together with EO bandwidths approaching approximately 200 GHz, demonstrating a favorable balance between modulation efficiency, propagation characteristics, and compact device operation.

Overall, the presented geometry-dependent framework provides useful design guidelines for future compact broadband graphene-enabled EO modulators requiring strong confinement, enhanced tunability, and energy-efficient operation.

Author Contributions: Conceptualization, A.G.A. and K.K.; methodology, A.G.A. and K.K.; validation, A.G.A.; formal analysis, A.G.A.; investigation, A.G.A.; resources, A.G.A. and K.K.; data curation, A.G.A.; writing—original draft preparation, A.G.A.; writing—review and editing, A.G.A. and K.K.; visualization, A.G.A. and K.K.; supervision, K.K.; project administration, K.K.; funding acquisition, K.K. All authors have read and agreed to the published version of the manuscript.

Funding: This research was funded by the National Institute of Information and Communications Technology (NICT), grant number JPJ012368C09801.

Data Availability Statement: The data supporting the findings of this study are available within the article. Further inquiries can be directed to the corresponding authors.

Conflicts of Interest: The authors declare no conflicts of interest.

References

1. Thomson, D.; Zilkie, A.; Bowers, J.E.; Komljenovic, T.; Reed, G.T.; Vivien, L.; Marris-Morini, D.; Cassan, E.; Virot, L.; Fédéli, J.M.; et al. Roadmap on silicon photonics. *J. Opt.* **2016**, *18*, 073003. [CrossRef]
2. Ye, W.N.; Xiong, Y. Review of silicon photonics: History and recent advances. *J. Mod. Opt.* **2013**, *60*, 1299–1320. [CrossRef]
3. Han, C.; Jin, M.; Tao, Y.; Shen, B.; Wang, X. Recent progress in silicon-based slow-light electro-optic modulators. *Micromachines* **2022**, *13*, 400. [CrossRef]
4. Wu, J.; Lin, H.; Moss, D.J.; Loh, K.P.; Jia, B. Graphene oxide for photonics, electronics and optoelectronics. *Nat. Rev. Chem.* **2023**, *7*, 162–183. [CrossRef]
5. Tang, H.; Menabde, S.G.; Anwar, T.; Kim, J.; Jang, M.S.; Tagliabue, G. Photo-modulated optical and electrical properties of graphene. *Nanophotonics* **2022**, *11*, 917–940. [CrossRef]
6. Datta, I. *Platform Based on Two-Dimensional (2D) Materials for Next-Generation Integrated Photonics*; Columbia University: New York, NY, USA, 2022.
7. Qiu, C.; Zeng, H.; Su, Y. Recent progress in graphene-based optical modulators on silicon photonics platform. *Natl. Sci. Open* **2022**, *1*, 20220031. [CrossRef]
8. Kasani, S.; Curtin, K.; Wu, N. A review of 2D and 3D plasmonic nanostructure array patterns: Fabrication, light management and sensing applications. *Nanophotonics* **2019**, *8*, 2065–2089. [CrossRef]
9. Kanwal, S.; Abdulsada, A.M.; Rezaei, M.H. High modulation depth, ultra-compact, and tunable electro-optical modulator based on dielectric-loaded graphene-plasmonic waveguides. *Opt. Lasers Eng.* **2025**, *193*, 109059. [CrossRef]
10. Maleki, M.; Soroosh, M.; Akbarizadeh, G. A compact low-loss 2-to-4 plasmonic decoder based on suspended graphene for surface plasmon polariton transmission. *Diam. Relat. Mater.* **2024**, *144*, 110983. [CrossRef]
11. Guo, Y.; Xu, Z.; Curto, A.G.; Zeng, Y.J.; Van Thourhout, D. Plasmonic semiconductors: Materials, tunability and applications. *Prog. Mater. Sci.* **2023**, *138*, 101158. [CrossRef]
12. Jin, M.; Wei, Z.; Meng, Y.; Shu, H.; Tao, Y.; Bai, B.; Wang, X. Silicon-based graphene electro-optical modulators. *Photonics* **2022**, *9*, 82. [CrossRef]

13. Zhang, Z.; Lee, Y.; Haque, M.F.; Leem, J.; Hsieh, E.Y.; Nam, S. Plasmonic sensors based on graphene and graphene hybrid materials. *Nano Converg.* **2022**, *9*, 28. [CrossRef] [PubMed]
14. Chauhan, D.; Sbeah, Z.; Dwivedi, R.P.; Nunzi, J.M.; Thakur, M.S. An investigation and analysis of plasmonic modulators: A review. *J. Opt. Commun.* **2024**, *45*, 483–511. [CrossRef]
15. Lin, C.C.C. Photonic Devices Using Coupled Plasmonic Structures. Ph.D. Thesis, University of Toronto (Canada), Toronto, ON, Canada, 2019.
16. Dubey, P.K.; Raju, A.I.; Lukose, R.; Wenger, C.; Lukosius, M. Optimizing graphene ring modulators: A comparative study of straight, bent, and racetrack geometries. *Nanomaterials* **2025**, *15*, 1158. [CrossRef]
17. Watson, H. Graphene Modulators for Silicon Photonic Optical Links. Ph.D. Thesis, University of Cambridge, Cambridge, UK, 2021.
18. Bian, Y.; Gong, Q. Highly confined guiding of low-loss plasmon waves in hybrid metal-dielectric slot waveguides. *Nanotechnology* **2014**, *25*, 345201. [CrossRef]
19. Zhao, Y.; Zhu, Y. Graphene-based hybrid films for plasmonic sensing. *Nanoscale* **2015**, *7*, 14561–14576. [CrossRef]
20. Amin, R.; George, J.K.; Wang, H.; Maiti, R.; Ma, Z.; Dalir, H.; Khurgin, J.B.; Sorger, V.J. An ITO–graphene heterojunction integrated absorption modulator on Si-photonics for neuromorphic nonlinear activation. *APL Photonics* **2021**, *6*, 120801. [CrossRef]
21. Malard, L.M.; Fai Mak, K.; Castro Neto, A.; Peres, N.; Heinz, T.F. Observation of intra-and inter-band transitions in the transient optical response of graphene. *New J. Phys.* **2013**, *15*, 015009. [CrossRef]
22. Rhouma, M.B. Modeling and Simulation of Composite Plasmonic Structures Based on Graphene and Metals. Ph.D. Thesis, Université Clermont Auvergne, Clermont-Ferrand, France, 2021.
23. Snyder, A.W.; Love, J.D. *Optical Waveguide Theory*; Chapman and Hall: London, UK, 1983; Volume 175.
24. Hunsperger, R.G. Optical waveguide modes. In *Integrated Optics: Theory and Technology*; Springer: Berlin/Heidelberg, Germany, 2009; pp. 17–31.
25. Oshina, I.; Spigulis, J. Beer–Lambert law for optical tissue diagnostics: Current state of the art and the main limitations. *J. Biomed. Opt.* **2021**, *26*, 100901. [CrossRef] [PubMed]
26. Reed, G.T.; Mashanovich, G.; Gardes, F.Y.; Thomson, D. Silicon optical modulators. *Nat. Photonics* **2010**, *4*, 518–526. [CrossRef]
27. Wu, Z.; Xu, Y. Design of a graphene-based dual-slot hybrid plasmonic electro-absorption modulator with high-modulation efficiency and broad optical bandwidth for on-chip communication. *Appl. Opt.* **2018**, *57*, 3260–3267. [CrossRef] [PubMed]
28. AlAloul, M.; Rasras, M. Low insertion loss plasmon-enhanced graphene all-optical modulator. *ACS Omega* **2021**, *6*, 7576–7584. [CrossRef]

Disclaimer/Publisher's Note: The statements, opinions and data contained in all publications are solely those of the individual author(s) and contributor(s) and not of MDPI and/or the editor(s). MDPI and/or the editor(s) disclaim responsibility for any injury to people or property resulting from any ideas, methods, instructions or products referred to in the content.